Resonant X-ray second harmonic generation in atomic gases

Ji-Cai Liu[1,2*], Catalin Miron[3,4,5], Hans Ågren[6,7],
Sergei Polyutov[8,9], and Faris Gel'mukhanov[6,8,9,10]

[1] *Department of Mathematics and Physics,*
North China Electric Power University,
102206 Beijing, China

[2] *Collaborative Innovation Center of Light Manipulations and Applications,*
Shandong Normal University,
Jinan 250358, China

[3] *Synchrotron SOLEIL,*
l'Orme des Merisiers,
Saint-Aubin, BP 48,
91192 Gif-sur-Yvette Cedex, France

[4] *Extreme Light Infrastructure Nuclear Physics (ELI-NP),*
'Horia Hulubei' National Institute for Physics and Nuclear Engineering,
30 Reactorului Street, RO-077125 Măgurele,
Judet Ilfov, Romania

[5] *LIDYL, CEA, CNRS,*
Université Paris-Saclay, CEA Saclay,
91191 Gif-sur-Yvette, France

[6] *Theoretical Chemistry & Biology,*
School of Biotechnology,
Royal Institute of Technology,
S-106 91 Stockholm, Sweden

[7] *Department of Physics and Astronomy,*
UppsalaUniversity,
SE-75120Uppsala, Sweden

[8] *Siberian Federal University,*

* jicailiu@ncepu.edu.cn

660041 Krasnoyarsk, Russia

[9] *Kirensky Institute of Physics,*

Federal Research Center KSC SB RAS,

660036 Krasnoyarsk, Russia

[10] *Institute for Methods and Instrumentation*

in Synchrotron Radiation Research FG-ISRR,

Helmholtz-Zentrum Berlin für Materialien und Energie Albert-Einstein-Strasse 15,

12489 Berlin, Germany

Abstract

We explore the X-ray second harmonic generation process induced by resonant two-photon absorption in systems with inversion symmetry. We show that this process becomes allowed in the X-ray region due to non-dipole contributions. It is found that while a plane wave pump field generates only a longitudinal second harmonic field, a Gaussian pump beam creates also a radially polarized transverse second harmonic field which is stronger than the longitudinal one. Contrary to the longitudinal component, the transverse second harmonic field with zero intensity on the axis of the pump beam can run in free space. Our theory is applied to Ar and Ne atomic vapours and predicts an energy conversion efficiency of X-ray SH generation of 3.2×10^{-11} and 1.3×10^{-12}, respectively.

I. INTRODUCTION

Modern X-ray Free Electron Laser (XFEL) facilities can deliver high intensities $10^{15}-10^{19}$ W/cm^2 making it possible to significantly populate a core-excited state and even create population inversion and X-ray lasing [1–7]. At these intensities, X-ray matter interaction becomes nonlinear creating room for studies of nonlinear effects like stimulated X-ray Raman scattering [3–5, 8–10], pulse compression [3–5], X-ray four-wave mixing [3–5, 11, 12], and nonlinear wave mixing of X-ray and near-infrared beams [13]. Special attention was paid to the competition between stimulated X-ray emission and Auger decay [14–16]. Second harmonic generation (SHG) is a nonlinear optical process of sum frequency generation which produces new photons with twice the frequency. SHG has traditionally been studied as an even-order nonlinear optical effect allowed in media without inversion symmetry[17] and is one of the best-understood nonlinear effects in optics[18]. In light of the XFEL development its study in the Angstrom regime, e.g., on the natural scale of atomic and molecular structure of matter, has become of great interest both from a fundamental and practical viewpoint. A pioneering study by Shwartz, Yudovich et al[19, 20] gave recently experimental evidence for "off-resonant" SHG in diamond in the hard X-ray region with a pump frequency of 7.3 keV.

In the present work we show that due to the large momentum of the photon $\mathbf{k}$ the nonlinearity in the X-ray region is different from conventional nonlinearities in the visible regime and that SHG is generally possible to observe for centro-symmetric systems even when phase matching conditions do not prevail. We present a theoretical study of X-ray SHG in atomic gases induced by resonant two-photon absorption (TPA). We show that the plane wave pump field can create only longitudinally polarised X-ray second harmonic (SH) fields which can not propagate in free space (see however ref.[21]), but also that a Gaussian pump pulse induces in addition transverse second harmonic fields which contrary to the longitudinal component can run in free space. Our idea is, in a certain sense, inverse to the use of the longitudinal component of focused light beams in laser particle accelerators[22]. Another important feature of the SHG problem studied here is that the transverse field, being strictly equal to zero on the beam axis, has an unusual radial polarization.

Our work is organized as follows. We outline in Sec. II A the basic theory of SHG using plane-wave pump radiation which generates only the longitudinal field. Then, in

the following Sec. II B we show that a Gaussian pump field creates also the transversely polarized SH field. Sec. II C is devoted to the analysis of the longitudinally and radially polarized SH fields. We shed light on the role of the absorption of an SH field in Sec. II D. Some theoretical details can be found in Appendixes A, B and C. We discuss our results further in Sec. III where we numerically analyze the efficiency of SHG in Ne and Ar vapours. Finally, in Sec. IV, we come to the conclusions.

II. THEORY

Quantum mechanically, the second order nonlinearity in the optical susceptibility originates from a perturbational solution of the Schrödinger's equation. To get insight into the physics of the SHG process in the X-ray region, we consider the propagation of an X-ray pump field $\mathbf{E}_p$ in an atomic gas far away from the absorption edge. To induce the SHG we choose twice the frequency of the pump field to be resonant with the frequency of a two-photon transition $2\omega \approx \omega_{10}$. The scheme of SHG is shown in Fig.1 where the pump field resonantly promotes the $1s$ electron of atom to the np unoccupied level. The resonant population of the state $|1\rangle$ in the course of TPA is followed by the emission of the SH field $\mathbf{E}$. Let us start from the atom-field interaction which reads as (we use SI units)

$$V = V^{(1)} + V^{(2)} = -\frac{e}{2mc}\left(\mathbf{p}\cdot\boldsymbol{\mathcal{A}}_p + \boldsymbol{\mathcal{A}}_p\cdot\mathbf{p}\right) + \frac{e^2}{2mc^2}\boldsymbol{\mathcal{A}}_p^2, \tag{1}$$

where m and e are the mass and charge of the electron, respectively. c is the speed of light and $\mathbf{p}$ is the operator of electronic momentum. Below we will use more frequently the electric field instead of the vector potential, $\boldsymbol{\mathcal{E}} = -\partial\boldsymbol{\mathcal{A}}/\partial t$. The square of the vector potential of the pump field $\boldsymbol{\mathcal{A}}_p^2$ describes the TPA process in the first order of perturbation theory while the scalar product $\mathbf{p}\cdot\boldsymbol{\mathcal{A}}_p$ contributes to the TPA in second order of perturbation theory.

A. Plane wave pump field

It is instructive to consider first the interaction with the simplest and most fundamental electromagnetic wave, the transverse plane wave $\boldsymbol{\mathcal{A}}_p = (\mathbf{A}_p/2)\exp(-\imath(\omega t - \mathbf{k}\cdot\mathbf{r} - \mathbf{k}\cdot\mathbf{r}^{(e)})) + c.c$

$$\begin{aligned}\boldsymbol{\mathcal{E}}_p &= \frac{1}{2}\mathbf{E}_p e^{-\imath(\omega t - \mathbf{k}\cdot\mathbf{r} - \mathbf{k}\cdot\mathbf{r}^{(e)})} + c.c.,\\ \mathbf{E}_p &= \mathbf{e}E_p^{(0)} = -\frac{\partial\mathbf{A}_p}{\partial t} = \imath\omega\mathbf{A}_p\end{aligned} \tag{2}$$

with the polarization $\mathbf{e}$ being orthogonal to the photon momentum $\mathbf{k}$. Here $\mathbf{r}^{(e)}$ is the coordinate of the electron with respect to the atom and $\mathbf{r}$ is the radius vector of atom in the laboratory frame. To avoid unnecessary complexity (see also below) we will focus only on the $\mathbf{A}_p^2$ term assuming that the wave length of the photon is longer than the size of the core orbital $ka \ll 1$

$$V^{(2)} = \frac{e^2}{8mc^2} A^2 e^{-\imath 2(\omega t - \mathbf{k}\cdot\mathbf{r}^{(e)} - \mathbf{k}\cdot\mathbf{r})} + c.c. + \text{const} \tag{3}$$
$$\approx \frac{e^2}{8mc^2} A_p^{(0)2} e^{-\imath 2(\omega t - \mathbf{k}\cdot\mathbf{r})}(1 + \imath 2\mathbf{k}\cdot\mathbf{r}^{(e)}) + c.c. + \text{const.}$$

The term $A_p^{(0)2}$ being independent on the electron radius vector $\mathbf{r}^{(e)}$ can not induce transitions between electronic states. Thus the transition between the ground (s) and core-excited (p) states is induced solely by the the matrix element

$$V_{10}^{(2)} \approx -\imath \frac{eE_p^{(0)2}}{4mc^2\omega^2}(\mathbf{k}\cdot\mathbf{d}_{10}) e^{-\imath[(2\omega-\omega_{10})t - 2\mathbf{k}\cdot\mathbf{r}]} \tag{4}$$

of the second term $\mathbf{k}\cdot\mathbf{r}^{(e)}$ on the right-hand side of eq.(3). The rotating-wave approximation is used here by keeping only the near resonant term. This pure non-dipole process opens the $s \to p$ TPA channel with the transition dipole moment $\mathbf{d}_{01} = e\mathbf{r}_{01} = e\langle 0|\mathbf{r}^{(e)}|1\rangle$ (Fig.1). We chose the axis z of quantization to lie along the photon momentum $\mathbf{k}$. In this frame the pump field populates only the np_z level (see Fig.1) and the problem is reduced to the interaction with a two-level atom with the transition dipole moment parallel to the photon momentum

$$\mathbf{d}_{01} \parallel \mathbf{k}. \tag{5}$$

The resonant TPA population of the core-excited state of p-symmetry is followed by the dipole allowed one-photon transition $p \to s$ which creates the SHG field with the double frequency 2ω. This explains why the SHG is possible in systems with inversion symmetry in the X-ray region.

To quantify the studied process one should compute the polarization $\boldsymbol{\mathcal{P}}$. The induced macroscopic polarisation of the medium being the expectation value of the dipole moment $\mathbf{d}$ is specified in terms of the density matrix $\rho(t)$

$$\boldsymbol{\mathcal{P}} = N\mathrm{Tr}(\mathbf{d}\rho) = N\left(\mathbf{d}_{01}(t)\rho_{10}(t) + \mathbf{d}_{10}(t)\rho_{01}(t)\right), \tag{6}$$

where N is the concentration of atoms and $\mathbf{d}_{01}(t) = \mathbf{d}_{01}\exp(\imath\omega_{10}t)$ is the dipole moment in the interaction representation[22, 23]. The off-diagonal element of the density matrix

$\rho_{10}(t) = \varrho_{10}\exp(-\imath(\nu t - 2\mathbf{k}\cdot\mathbf{r}))$ satisfies the following kinetic equation in the interaction picture[23]

$$\left(\frac{\partial}{\partial t} + \Gamma - \imath\nu\right)\varrho_{10} = \frac{1}{\hbar m}\Big(\frac{eE_p^{(0)}}{2\omega}\Big)^2(\mathbf{k}\cdot\mathbf{r}_{10})\left(\rho_{11} - \rho_{00}\right), \tag{7}$$

where $\nu = 2\omega - \omega_{10}$ is the detuning from the two-photon resonance and Γ is the lifetime broadening of core-excietd state $|1\rangle$. We neglect the very weak depopulation of the ground state in the course of the two-photon absorption, ($\rho_{00} \approx 1$, $\rho_{11} \ll 1$) and assume that the duration τ of the pump pulse is longer than the lifetime of the core excited state $1/\Gamma$. In this case one can use the stationary solution of eq.(7)

$$\varrho_{10} = \varrho_{01}^* = -\frac{1}{\hbar m}\left(\frac{eE_p^{(0)}}{2\omega}\right)^2\frac{(\mathbf{k}\cdot\mathbf{r}_{10})}{\Gamma - \imath\nu} \tag{8}$$

to find the induced macroscopic polarization taking into account eq.(5)

$$\begin{aligned}
&\boldsymbol{\mathcal{P}} = \mathbf{P}\; e^{-\imath 2(\omega t - \mathbf{k}\cdot\mathbf{r})} + c.c., \\
&\mathbf{P} = \hat{\mathbf{k}}p, \quad p = -\left(\frac{eE_p^{(0)}}{2\omega}\right)^2\frac{Nker_{01}^2}{m\hbar(\Gamma - \imath\nu)}.
\end{aligned} \tag{9}$$

Here $\hat{\mathbf{k}} = \mathbf{k}/k$ is the unit vector along $\mathbf{k}$. One can see that the pump radiation creates a macroscopic polarization $\boldsymbol{\mathcal{P}}$ oriented along the direction of propagation of the pump field $\mathbf{k}$, and hence the SH field $\boldsymbol{\mathcal{E}}$, which is created in the course of the spontaneous transition $|1\rangle \to |0\rangle$, is also parallel to $\mathbf{k}$. This longitudinal field exists everywhere where there is pump field and the medium and this field copies exactly the polarization according to Maxwell's equation for the induction, $\boldsymbol{\nabla}\cdot\boldsymbol{\mathcal{D}} = \partial(\epsilon_0\mathcal{E} + \mathcal{P})/\partial z = 0$:

$$\mathbf{E} = -\frac{2}{\epsilon_0}\mathbf{P} \neq 0, \quad \boldsymbol{\mathcal{D}} = 0, \quad \boldsymbol{\mathcal{H}} = 0. \tag{10}$$

This does not contradict the well known fact that the plane wave longitudinal field does not exist in free space[21]. This statement means that the longitudinal field can not propagate in free space. The longitudinal field $\boldsymbol{\mathcal{E}}$ exists only in the region where the pump field creates longitudinal polarization $\boldsymbol{\mathcal{P}} \propto \mathbf{k}$. This longitudinal field oscillating in time and space is a pure electric field, $\boldsymbol{\mathcal{H}} = 0$.

As we have already noticed above the TPA process is a first-order process with respect to $\boldsymbol{\mathcal{A}}_p^2$ and a second-order process with respect to $\mathbf{p}\cdot\boldsymbol{\mathcal{A}}_p$. Here we study the two-photon transition $s \to p$ which is a pure non-dipole effect. Since both $\boldsymbol{\mathcal{A}}_p^2$ and $\mathbf{p}\cdot\boldsymbol{\mathcal{A}}_p$ induced TPA

result in the same orientation of the TPA induced polarization we consider here only the $\boldsymbol{\mathcal{A}}_p^2$ contribution. The taking into account of the $\mathbf{p}\cdot\boldsymbol{\mathcal{A}}_p$ TPA process will result only in a rescaling of the SHG efficiency.

B. Gaussian pump beam and paraxial equation

In this section we will show that a Gaussian pump beam

$$\boldsymbol{\mathcal{E}}_p = \frac{1}{2}\mathbf{E}_p e^{-\imath(\omega t - kz)} + c.c., \tag{11}$$
$$\mathbf{E}_p = \hat{\mathbf{x}} E_p^{(0)} g\left(t - \frac{z}{c}\right)\frac{w_0}{w(z)}\exp\left(-\frac{\varrho^2}{w^2(z)}\right)\exp\left(\imath\left(k\frac{\varrho^2}{2R(z)} - \psi(z)\right)\right)$$

makes it possible to transform the longitudinal SHG X-ray field into a transfer field which can propagate in free space in contrast to the pure longitudinal field. Eq. (11) for pulsed Gaussian beam is obtained in Appendix A by convoluting of the fundamental Gaussian mode with the Gaussian distribution of spectral components. As shown in Appendix A, $\mathbf{E}_p$ satisfies paraxial equation. Eq.(11) identifies $R(z) = z\left(1 + (z_R/z)^2\right)$ as the radius of curvature of the wavefront of the beam at z, w_0 as the beam waist and $g(t) = \exp(-t^2/2\tau^2)$ as the temporal shape of the pulse with duration τ. Here $w(z) = w_0\sqrt{1+(z/z_R)^2}$, $\psi(z) = \arctan(z/z_R)$, $\rho = \sqrt{x^2+y^2}$, $w_0/z_R \sim 1/kw_0 \ll 1$. The Gaussian beam remains well collimated up to the Rayleigh range $z_R = kw_0^2/2$ (Fig.2).

Since the wavefront is not orthogonal to z, as one can see from the phase $\phi = 2k(z+\rho^2/2R)$ of $\mathcal{E}_p^2 \propto \exp(\imath\phi)$, the polarization $\mathbf{P}$ is slightly tilted from the z-axis. To find the matrix element $V_{01}^{(2)}$ of the interaction with the Gaussian pump beam (11) we need the value of this interaction at the point of the electron $\mathbf{r}^{(e)}$ with respect to the atom $\mathbf{r} = (\boldsymbol{\rho}, z)$, namely at $\mathbf{r} + \mathbf{r}^{(e)}$,

$$\langle 0|e^{\imath(\phi+\delta\phi)}|1\rangle \approx e^{\imath\phi}\langle 0|1 + \imath\delta\phi|1\rangle = \boldsymbol{\kappa}\cdot\langle 0|\mathbf{r}^{(e)}|1\rangle e^{\imath\phi}\,\imath 2k, \tag{12}$$

where we used the Taylor expansion $\phi(\mathbf{r}+\mathbf{r}^{(\mathbf{e})}) = \phi(\mathbf{r}) + \delta\phi$ with $\delta\phi = \boldsymbol{\nabla}\phi\cdot\mathbf{r}^{(e)}$. Similar to the derivation of eq.(9) one obtains a polarisation that is oriented along $\boldsymbol{\nabla}\phi \equiv (\partial_z\phi, \partial_\rho\phi) = 2k\boldsymbol{\kappa}$

$$\mathbf{P} = -\boldsymbol{\kappa}\left(\frac{eE_p}{2\omega}\right)^2 \frac{Nker_{01}^2}{m\hbar(\Gamma - \imath\nu)}, \quad \boldsymbol{\kappa} = \hat{\mathbf{z}} + \hat{\boldsymbol{\rho}}\frac{\rho}{R} \tag{13}$$

instead of the beam axis $\hat{\mathbf{z}} \parallel \mathbf{k}$.

Let us write the optical wave equation for the SHG field $\boldsymbol{\mathcal{E}}$

$$\boldsymbol{\nabla}(\boldsymbol{\nabla}\cdot\boldsymbol{\mathcal{E}}) - \boldsymbol{\nabla}^2\boldsymbol{\mathcal{E}} + \frac{1}{c^2}\frac{\partial^2\boldsymbol{\mathcal{E}}}{\partial t^2} = -\mu_0\frac{\partial^2\boldsymbol{\mathcal{P}}}{\partial t^2} \tag{14}$$

in the usual manner[18] starting from the couple of Maxwell's equations (in SI units) for nonmagnetic materials (μ=1)

$$\boldsymbol{\nabla} \times \boldsymbol{\mathcal{E}} = -\mu_0 \frac{\partial \boldsymbol{\mathcal{H}}}{\partial t}, \quad \boldsymbol{\nabla} \times \boldsymbol{\mathcal{H}} = \frac{\partial \boldsymbol{\mathcal{D}}}{\partial t}. \tag{15}$$

Contrary to conventional theories[18] where $\boldsymbol{\nabla} \cdot \boldsymbol{\mathcal{E}} \sim (\mathbf{k} \cdot \mathbf{e}) = \mathbf{0}$ for the transverse electromagnetic field ($\mathbf{k} \perp \mathbf{e}$), we can not ignore $\boldsymbol{\nabla} \cdot \boldsymbol{\mathcal{E}}$ here. This is because the polarization $\boldsymbol{\mathcal{P}}$ is essentially a longitudinal one (see eq.(13)): $\boldsymbol{\nabla} \cdot \boldsymbol{\mathcal{P}} \neq 0$. To resolve this problem we use the Maxwell's equation for the induction $\boldsymbol{\mathcal{D}} = \varepsilon_0 \boldsymbol{\mathcal{E}} + \boldsymbol{\mathcal{P}}$

$$\boldsymbol{\nabla} \cdot \boldsymbol{\mathcal{D}} = 0, \quad \boldsymbol{\nabla} \cdot \boldsymbol{\mathcal{E}} = -\frac{1}{\epsilon_0} \boldsymbol{\nabla} \cdot \boldsymbol{\mathcal{P}}, \tag{16}$$

which makes it possible to rewrite the wave equation (14) as follows

$$-\boldsymbol{\nabla}^2 \boldsymbol{\mathcal{E}} + \frac{1}{c^2} \frac{\partial^2 \boldsymbol{\mathcal{E}}}{\partial t^2} = \frac{1}{\epsilon_0} \left(-\frac{1}{c^2} \frac{\partial^2 \boldsymbol{\mathcal{P}}}{\partial t^2} + \boldsymbol{\nabla}(\boldsymbol{\nabla} \cdot \boldsymbol{\mathcal{P}}) \right), \tag{17}$$

$$\boldsymbol{\mathcal{E}} = \frac{1}{2} \mathbf{E} e^{-\imath 2(\omega t - kz)} + c.c., \quad \boldsymbol{\mathcal{P}} = \mathbf{P} e^{-\imath 2(\omega t - kz)} + c.c..$$

This wave equation differs from the conventional one [18] by the extra term $\boldsymbol{\nabla}(\boldsymbol{\nabla} \cdot \boldsymbol{\mathcal{P}}) \neq 0$ which is not equal to zero because of the longitudinal contribution in $\boldsymbol{\mathcal{P}}$. We would like to point out that when the pump field is a plane wave there is only a longitudinal SH field $\boldsymbol{\mathcal{E}} \parallel z$ (see Sec.II A). In this case the wave equation (14) becomes $\partial^2(\epsilon_0 \boldsymbol{\mathcal{E}} + \boldsymbol{\mathcal{P}})/\partial t^2 = 0$, which is very different from eq.(17) because $\boldsymbol{\nabla}(\boldsymbol{\nabla} \cdot \boldsymbol{\mathcal{E}}) - \boldsymbol{\nabla}^2 \boldsymbol{\mathcal{E}} = (\partial^2/\partial z^2 - \partial^2/\partial z^2)\mathcal{E} \equiv 0$.

Now we are at the stage to simplify the wave equation (17). In our case the wave propagates primarily along the z-axis with a small divergence angle (Fig. 2)

$$\theta_0 \approx \frac{1}{2kw_0} = \frac{w_0}{z_R} \sim \frac{\lambda}{w_0} \ll 1. \tag{18}$$

Here λ is the wavelength of the pump field. We assume also that the pulse duration τ is much longer than the period of field oscillations $2\pi/\omega$. This makes it possible to neglect $\partial^2 \mathbf{E}/\partial z^2$ and $\partial^2 \mathbf{E}/\partial t^2$ in eq. (17) (see Ref. [24]) and to get the following paraxial equation for the SHG field

$$\left(\frac{\partial}{\partial z} + \frac{1}{c} \frac{\partial}{\partial t} - \frac{\imath}{4k} \Delta_\perp \right) \mathbf{E} = \frac{\imath}{2k} \mathbf{f}, \quad kw_0 \gg 1, \quad \tau\omega \gg 1, \tag{19}$$

where $\Delta_\perp = \boldsymbol{\nabla}_\rho^2 = \partial^2/\partial x^2 + \partial^2/\partial y^2$ is the Laplacian operator over the transverse cartesian coordinates. The source term on the right-hand side of the paraxial equation has now both

longitudinal (f_z) and transverse components (f_ρ)

$$\begin{aligned}
&\tilde{\mathbf{f}} = \hat{\mathbf{z}}\tilde{f}_z + \hat{\boldsymbol{\rho}}\tilde{f}_\rho, \\
&\tilde{\mathbf{f}} = \frac{1}{\epsilon_0}\left(-\frac{1}{c^2}\frac{\partial^2\tilde{\mathbf{P}}}{\partial t^2} + \boldsymbol{\nabla}(\boldsymbol{\nabla}\cdot\tilde{\mathbf{P}})\right) \approx \frac{1}{\epsilon_0}\left((2k)^2\tilde{\mathbf{P}} + \boldsymbol{\nabla}(\boldsymbol{\nabla}\cdot\tilde{\mathbf{P}})\right), \\
&\tilde{\mathbf{P}} = \mathbf{P}e^{-\imath 2(\omega t - kz)}, \quad \tilde{\mathbf{f}} = \mathbf{f}e^{-\imath 2(\omega t - kz)}
\end{aligned} \tag{20}$$

Taking into account eqs.(11), (13) and (18) one can get the following expression for the transverse and longitudinal components of $\mathbf{f}$

$$\begin{aligned}
f_\rho &= -\frac{\imath 8k\rho}{\epsilon_0 w^2}P, \\
f_z &= \frac{\imath 2kP}{\epsilon_0(z^2+z_R^2)}\Big[\frac{2k\rho^2 z_R(\imath z_R + z)}{z^2+z_R^2} - \imath 4z_R - z\Big].
\end{aligned} \tag{21}$$

One should point out that the origin of the f_ρ is the term $\boldsymbol{\nabla}(\boldsymbol{\nabla}\cdot\tilde{\mathbf{P}}) = \hat{\boldsymbol{\rho}}\partial_\rho(\partial_z\tilde{P}) + \cdots$. A simple estimation shows that the transverse contribution dominates: $|f_\rho/f_z| \sim kw_0 \gg 1$. As one can see from the paraxial equation (19) the transverse and longitudinal components of $\mathbf{f}$ generate, respectively, the transverse and longitudinal components of the SH field $\mathbf{E}$.

C. Spatial distribution of the transverse and longitudinal SH fields. Radial polarization

It is convenient to write the solution of the paraxial equation (19) in terms of the retarded Green's function (see Appendix B)

$$\begin{aligned}
&\mathbf{E}(z,\boldsymbol{\rho},t) = \frac{1}{2\pi}\int G(z-z',\boldsymbol{\rho}-\boldsymbol{\rho}',t-t')\mathbf{f}(z',\boldsymbol{\rho}',t')dz'd\boldsymbol{\rho}'dt', \\
&\left(\frac{\partial}{\partial z} + \frac{1}{c}\frac{\partial}{\partial t} - \frac{\imath}{4k}\Delta_\perp\right)G(z-z',\boldsymbol{\rho}-\boldsymbol{\rho}',t-t') = \delta(z-z')\delta(\boldsymbol{\rho}-\boldsymbol{\rho}')\delta(t-t')\Theta(t-t'). \\
&G(z-z',\boldsymbol{\rho}-\boldsymbol{\rho}',t-t') = -\imath\delta\left(t'-t-\frac{z'-z}{c})\right)\Theta(t-t')\frac{k}{\pi(z-z')}\exp\left(\imath\frac{k|\boldsymbol{\rho}-\boldsymbol{\rho}')^2}{z-z'}\right),
\end{aligned} \tag{22}$$

which guarantees that no contribution at remotely early times, t, before the source $\tilde{\mathbf{f}}(z',\boldsymbol{\rho}',t') = \mathbf{f}(z',\boldsymbol{\rho}',t')\exp(-\imath 2(\omega t' - kz'))$ has been activated. Taking into account that $\hat{\mathbf{z}}' = \hat{\mathbf{z}}$, $\hat{\boldsymbol{\rho}}' = \hat{\boldsymbol{\rho}}\cos\varphi + \hat{\mathbf{y}}\sin\varphi$, $\hat{\mathbf{y}} \perp \hat{\boldsymbol{\rho}}$, one can perform an integration over directions of $\boldsymbol{\rho}'$ in

the plane $(\hat{\boldsymbol{\rho}}, \hat{\mathbf{y}})$ orthogonal to the z-axis using eq.(B5)

$$\int_0^{2\pi} d\varphi[\hat{\boldsymbol{\rho}}' f_\rho(z', \rho', t') + \hat{\mathbf{z}} f_z(z', \rho', t')] \exp\left(\imath \frac{k|\boldsymbol{\rho} - \boldsymbol{\rho}')^2}{z - z'}\right) \tag{23}$$
$$= 2\pi \exp\left(\imath \frac{k(\rho^2 + \rho'^2)}{z - z'}\right) \Big[- \hat{\boldsymbol{\rho}} \imath f_\rho(z', \rho', t') J_1\left(\frac{2k\rho\rho'}{z - z'}\right) + \hat{\mathbf{z}} f_z(z', \rho', t') J_0\left(\frac{2k\rho\rho'}{z - z'}\right) \Big],$$

where $J_n(x)$ is a Bessel function. One can obtain the remaining integral over ρ' using eq.(B5) and get the following expressions for transverse and longitudinal contributions

$$\mathbf{E}(z, \boldsymbol{\rho}, t) = \hat{\boldsymbol{\rho}} E_\rho(z, \boldsymbol{\rho}, t) + \hat{\mathbf{z}} E_z(z, \boldsymbol{\rho}, t), \tag{24}$$
$$E_i(z, \rho, t) = E_p^{(0)} g^2\left(t - \frac{z}{c}\right) J_i(z, \rho), \quad i = (\rho, z),$$

where

$$J_\rho(z, \rho) = -2\rho s_0 \int_{-\infty}^{z} dz' \frac{e^\Phi}{w^4(z')\alpha^2(z')}, \tag{25}$$
$$J_z(z, \rho) = \frac{\imath 4\pi w_0 s_0}{(k w_0)^3} \int_{-\infty}^{z} dz' \frac{e^\Phi}{w^4(z')\alpha(z')} \left[\frac{2(\imath z_R + z')}{w^2(z')\alpha(z')}\left(z - z' - \frac{2k^2\rho^2}{\alpha(z')}\right) - (\imath 4 z_R + z')\right],$$
$$\Phi = \frac{\imath k\rho^2}{z - z'} - \imath 2\psi(z') - \frac{k^2\rho^2}{(z - z')\alpha(z')}, \quad \alpha(z') = \frac{2(z - z')}{w^2(z')} - \imath k\left(\frac{z - z'}{R(z')} + 1\right),$$
$$s_0 = 8\pi \frac{G}{\Gamma - \imath\nu} N z_R r_{01} r_e$$

Here $r_e = e^2/(4\pi\epsilon_0 mc^2) = 2.82 \times 10^{-13}$ cm is the classical electron radius and $G = E_p^{(0)} d_{01}/\hbar$ is the Rabi frequency. It is important to notice that there is no transverse field on the beam axis

$$E_\rho(z, \rho = 0, t) = 0. \tag{26}$$

Eq.(24) indicates that the transverse SH field $\hat{\boldsymbol{\rho}} E_\rho$ is oriented along the radius $\boldsymbol{\rho}$ perpendicular to the beam axis (Fig. 3). This means that the transverse field has radial polarization (see also Sec. III).

D. Role of photoabsorption

In the equations above the photoabsorpion of X-rays is ignored. This approximation is valid for the pump beam whose frequency is far from any resonance. In contrast, the SHG

field is in strict resonance with the dipole allowed transition $|0\rangle \to |1\rangle$ ($1s-3p$ for Ne and $1s-4p$ for Ar). Therefore, this absorption channel should be taken into account. With the solution (24) at hand we are almost prepared to include the photoabsorption in the SH field. As shown in Appendix C the photoabsorption of the SHG field modifies only the integrands at the right-hand side of equations (25) for $J_\rho(z,\rho)$ and $J_z(z,\rho)$. Namely, these integrands should be multiplied by the factor

$$\exp\left(\frac{z'-z}{2\ell}\right), \tag{27}$$

where $\ell = 1/N\sigma_{\rm abs}$ is the photoabsorption length while $\sigma_{\rm abs}$ is the resonant photoabsorption cross section. According to simulations the photoabsorption length should be larger or comparable with the Rayleigh range

$$\ell \sim z_R \tag{28}$$

to make it possible for the SHG field to reach the optimal value.

III. RESULTS OF SIMULATIONS AND DISCUSSION

We applied the theory outlined above to two atomic systems, Ne and Ar, under the strict two-photon resonance ($2\omega = \omega_{10}$) with $1s \to 3p$ transitions for Ne and $1s \to 4p$ transitions for Ar. In the simulations, the peak pump intensity used was $I_p^{(0)} = c\epsilon_0|E_p^{(0)}|^2/2 = 10^{16}$ W/cm^2 (Fig. 2), and the following parameters were adopted for Ne: $\hbar\omega_{1s-3p} = 867.4$ eV, $\sigma_{\rm abs}(1s-3p) = 1.5\times10^{-18}$ cm^2[25], $2\hbar\Gamma = 0.27$ eV [26], and for Ar: $\hbar\omega_{1s-4p} = 3203.42$ eV, $\sigma_{\rm abs}(1s-4p) = 0.12\times10^{-18}$ cm^2[27], $2\hbar\Gamma = 0.66$ eV[28]. The concentration of the atoms and the beam waist were equal to $N = 10^{19}$ cm^{-3} and $w_0 = 1.0\mu$m, respectively. The Rayleigh range was $z_R \approx 10^3\mu$m and $z_R \approx 4\times10^3\mu$m for Ne and Ar, respectively. The corresponding values of the photoabsorption lengths $\ell \approx 0.67\times10^3\mu$m and $8\times10^3\mu$m satisfy the condition (28).

We solved the paraxial equation with homogeneous distribution of the concentration. The SHG radiation is characterized by the intensity distributions of the transverse ($I_\rho(z,\rho,t)$) and longitudinal ($I_z(z,\rho,t)$) components of the SH field (24)

$$I_i(z,\rho,t) = \frac{1}{2}c\epsilon_0|E_i(z,\rho,t)|^2, \quad i = (\rho,z) \tag{29}$$

and by the energy conversion efficiency

$$\beta_i = \frac{W_i(z)}{W_p}, \quad W_i(z) = 2\pi \int_0^\infty dt \int_0^{2\pi} d\rho I_i(z,\rho,t). \tag{30}$$

First we studied the SH field neglecting the photoabsorption. In Fig. 4 and Fig. 5 we display the spatial distribution of the SH intensities $I_\rho(z,\rho,t)$ and $I_z(z,\rho,t)$ for Ne and Ar, respectively. One can see that the transverse and longitudinal SH fields show very different radial structures with $I_\rho = 0$ on the axis of the beam $\rho = 0$, and the transverse field $\hat{\boldsymbol{\rho}} E_\rho$ (24) has an unusual radial polarization as shown in Fig. 3. The transverse SH field I_ρ is much stronger than the longitudinal one I_z, and the energy conversion efficiency of the transverse SH field is about four to five orders of magnitude larger than that of the longitudinal SH field as shown in Fig. 6.

Because of the deeper ionization potential and smaller core-electron transition dipole moment, the conversion efficiencies of the X-ray SH fields from Ar atomic vapour are much smaller than those from Ne (Fig. 6). However, when the photoabsorption of the generated SH fields is considered, the final conversion efficiencies from Ar and Ne become comparable. Below we investigated the conditions for the experimental observation of the SHG process with X-rays in atomic Ne and Ar vapours by taking into account the resonant one-photon absorption of the SH field during propagation. The photoabsorption changes the spatial distribution of the SH field (Fig. 7) and reduces the energy conversion efficiency in one order of magnitude for Ne and in four times for Ar, as one can see from Fig. 6 and Fig.8. As it is expected the SH field is confined in the focal region in the range limited by the photoabsorption length ℓ (see Fig. 7). Due to this circumstance the energy conversion efficiency becomes maximal at $z = z_{\max} = 0.7$ mm for Ne and $z_{\max} = 0.5$ cm for Ar. This range defines the size of the gas cell which should be around $z_{\max}$.

IV. SUMMARY

In this paper, we investigated the second harmonic generation in systems with inversion symmetry in the X-ray region. Our theory is applied to SHG in neon and argon pumped by a strong X-ray field tuned in resonance with the two-photon transition $1s \to 3p$ in Ne and $1s \to 4p$ in Ar. The non-dipole population of these core-excited states is followed by the emission of the SH field. We describe the SHG in atoms in terms of a density

matrix formalism and paraxial equation taking into account the resonant photoabsorption of the SH radiation. In contrast to the plane wave pump field, the Gaussian pump beam generates transverse SH photons with radial polarization. By taking into account the X-ray photoabsorption effect, the energy conversion efficiencies to the transverse SH fields are expected to be orders of 10^{-11} and 10^{-12} in Ne (867.4 eV) and Ar (3203.4 eV) atomic vapours for the pump 10^{16} W/cm^2, respectively.

Acknowledgements. The research leading to these results has received funding from a public grant from the Laboratoire d'Excellence Physics Atoms Light Matter (LabEx PALM), the Laboratoire d'Excellence MiChEm, and the Swedish Research Council (VR). JL thanks the support by the National Science Foundation of China under grant Nos. 11574082 and 11974108, and the Fundamental Research Funds for the Central Universities under grant No. 2018MS050. FG and SP acknowledge support within the State contract of the Russian Federation Ministry of Education and Science for Siberian Federal University for scientific research in 2017-2019 (Project 3.2662.2017). HÅ acknowledges the Knut and Alice Wallenberg foundation for financial support (Grant No. KAW-2013.0020).

Appendix A: The pulsed Gaussian beam (11) is eigen function of paraxial operator

To get pulsed Gaussian beam (11) with the carrier frequency ω we need to convolute fundamental Gaussian mode

$$\boldsymbol{\mathcal{E}}(\omega,t)=\frac{1}{2}\mathbf{E}(\omega)e^{-\imath(\omega t-kz)}+c.c., \tag{A1}$$
$$\mathbf{E}(\omega)=\hat{\mathbf{x}}E_p^{(0)}\frac{w_0}{w_(z)}\exp\left(-\frac{\varrho^2}{w^2(z)}\right)\exp\left(\imath\left(k\frac{\varrho^2}{2R(z)}-\psi(z)\right)\right),$$

with the spectral distribution $g(\omega'-\omega)=\exp(-(\omega'-\omega)^2\tau^2/2)/\tau\sqrt{2\pi}$ centered at the carrier frequency ω

$$\boldsymbol{\mathcal{E}}_p(\omega,t)=\int_{-\infty}^{\infty}g(\omega'-\omega)\boldsymbol{\mathcal{E}}(\omega',t)d\omega'. \tag{A2}$$

The mode $\mathbf{E}(\omega)$ is the eigen function of the stationary paraxial or Helmholtz equation

$$\left(\frac{\partial}{\partial z}-\frac{\imath}{2k}\Delta_\perp\right)\mathbf{E}(\omega)=0. \tag{A3}$$

The substitution of the fundamental mode (A1) in the convolution (A2) results in an expression

$$\boldsymbol{\mathcal{E}}_p(\omega,t)=\frac{\hat{\mathbf{x}}}{2}E_p^{(0)}\int\limits_{-\infty}^{\infty}d\omega' g(\omega'-\omega)$$

$$\times\exp\left(-\imath\omega'\left(t-\frac{z}{c}-\frac{\rho^2}{2cR(z)}\right)\right)\frac{w_0}{w(z)}\exp\left(-\frac{\varrho^2}{w^2(z)}\right)e^{-\imath\psi(z)}+c.c. \tag{A4}$$

We neglect the ω'-dependence of the Rayleigh range $z_R=k'w_0^2/2\approx kw_0^2/2$ because the variation of the frequency $\Delta\omega=|\omega'-\omega|\sim 1/\tau$ in the Fourier transform (A4) is negligibly small in comparison with the carrier frequency of X-ray pulse: $\Delta\omega/\omega\sim 1/\tau\omega\ll 1$. Thus

$$\boldsymbol{\mathcal{E}}_p(\omega,t)\approx\frac{\hat{\mathbf{x}}}{2}E_p^{(0)}\exp\left(-\imath\omega\left(t-\frac{z}{c}-\frac{\rho^2}{2cR(z)}\right)\right)\frac{w_0}{w(z)}\exp\left(-\frac{\varrho^2}{w^2(z)}\right)e^{-\imath\psi(z)}$$

$$\times g\left(t-\frac{z}{c}-\frac{\rho^2}{2cR(z)}\right)+c.c.,\quad g(t)=\exp\left(-\frac{t^2}{2\tau^2}\right) \tag{A5}$$

Within paraxial approximation [24] ($kw_0\gg 1$) we can neglect $\rho^2/2cR(z)$ in the Gaussian $g\left(t-z/c-\rho^2/2cR(z)\right))$ because

$$z\sim z_R\sim kw_0^2\gg\frac{\rho^2}{2R(z)}\sim\frac{w_0^2}{z_R}\sim\frac{1}{k},\quad\frac{\rho^2}{2cR(z)\tau}\sim\frac{1}{\tau\omega}\ll 1. \tag{A6}$$

However, we should keep $\rho^2/2cR(z)$ in the oscillatory term $\exp[-\imath\omega(t-z/c-\rho^2/2cR(z))]$ because

$$\omega\frac{\rho^2}{2cR(z)}=\frac{k\rho^2}{2R(z)}\approx\frac{kw_0^2}{2z_R}\sim 1. \tag{A7}$$

Finally we get eq.(11) for $\boldsymbol{\mathcal{E}}_p(\omega,t)$.

Now we are in stage to show that $\mathbf{E_p}$ from eq.(11) satisfies the paraxial equation

$$\left(\frac{\partial}{\partial z}+\frac{1}{c}\frac{\partial}{\partial t}-\frac{\imath}{2k}\Delta_\perp\right)\mathbf{E_p}=0. \tag{A8}$$

Let us apply the operator $\Box=-\nabla^2+\partial^2/c^2\partial^2 t$ to both sides of eq.(A2)

$$\Box\boldsymbol{\mathcal{E}}_p(\omega,t)=\int\limits_{-\infty}^{\infty}g(\omega'-\omega)\Box\boldsymbol{\mathcal{E}}(\omega',t)d\omega'. \tag{A9}$$

Using the paraxial approximation, $kw_0\gg 1$, $\tau\omega\gg 1$ and eq.(A3) we get eq.(A8)

$$\left(\frac{\partial}{\partial z}+\frac{1}{c}\frac{\partial}{\partial t}-\frac{\imath}{2k}\Delta_\perp\right)\mathbf{E_p}=e^{\imath(\omega t-kz)} \tag{A10}$$

$$\times\int\limits_{-\infty}^{\infty}d\omega' g(\omega'-\omega)\frac{k'}{k}e^{-\imath(\omega' t-k'z)}\left(\frac{\partial}{\partial z}-\frac{\imath}{2k'}\Delta_\perp\right)\mathbf{E}(\omega')=0. \tag{A11}$$

The paraxial approximation is broken when $kw_0 \lesssim 1$, $\tau\omega \lesssim 1$. In this case one should restore in eq. (19) the second derivatives over z and time: $\partial/\partial z \to \partial/\partial z - (\imath/4k)\partial^2/\partial z^2$, $\Delta_\perp \to \Delta_\perp - \partial^2/c^2\partial t^2$. However, such conditions are difficult to reach in X-ray region. For example, the condition $\tau\omega \sim 1$ corresponds to few cycle X-ray pulse, where the pulse duration is comparable with the period of the field oscillations.

Appendix B: Green's function for the time-dependent paraxial equation

Let us find the Green's function of non-stationary paraxial equation

$$\left(\frac{\partial}{\partial z} + \frac{1}{c}\frac{\partial}{\partial t} - \frac{\imath}{2K}\Delta_\perp\right) G(z, \boldsymbol{\rho}, t) = \Theta(t)\delta(t)\delta(z)\delta(\boldsymbol{\rho}), \tag{B1}$$

where $\Delta_\perp = \partial^2/\partial x^2 + \partial^2/\partial y^2$, $\boldsymbol{\rho} = (x, y)$, $\delta(\boldsymbol{\rho}) = \delta(x)\delta(y)$ and $\Theta(t)$ is the step function which is equal to zero when $t < 0$. Taking the Fourier transform of the Green's function and of the Dirac δ-functions we get

$$\begin{aligned} G(z, \boldsymbol{\rho}, t) &= \frac{\Theta(t)}{(2\pi)^4} \int\limits_{-\infty}^{\infty} d\mu \int\limits_{-\infty}^{\infty} d\nu \int\limits_{-\infty}^{\infty} dp \int\limits_{-\infty}^{\infty} dq G_{\mu,\nu,p,q} e^{\imath\mu t + \imath\nu z + \imath p x + \imath q y}, \\ G_{\mu,\nu,p,q} &= -\frac{2\imath}{\frac{\mu}{c} + \nu + \frac{p^2+q^2}{2K}}. \end{aligned} \tag{B2}$$

Keeping in mind that $t \geq 0$ and taking the integral along half circle in upper half plane around the pole $\mu = -c\left(\nu + \frac{p^2+q^2}{2K}\right)$

$$\int\limits_{-\infty}^{\infty} \frac{e^{\imath\mu t}}{\frac{\mu}{c} + \nu + \frac{p^2+q^2}{2K}} d\mu = -\imath c\pi \exp\left(-\imath c t\left(\nu + \frac{p^2+q^2}{2K}\right)\right), \tag{B3}$$

we obtain the following expression for the Green's function

$$G(z, \boldsymbol{\rho}, t) = -\imath\delta\left(t - \frac{z}{c}\right)\Theta(t)\frac{K}{2\pi z}\exp\left(\imath\frac{K\rho^2}{2z}\right) \tag{B4}$$

which allows to find the SHG field (22) with help of the following integrals[29]

$$\begin{aligned} &J_0(a) = \frac{1}{2\pi}\int_0^{2\pi} e^{\imath a\cos\theta} d\theta, \\ &\frac{1}{2\pi}\int_0^{2\pi} \cos\theta e^{-\imath a\cos\theta} d\theta = \imath\frac{d}{da}J_0(a) = -\imath J_1(a), \\ &\int\limits_0^{\infty} e^{-a^2\rho^2}\rho^{n+1}J_n(b\rho)d\rho = \frac{b^n}{(2a^2)^{n+1}}e^{-\frac{b^2}{4a^2}}, \quad \mathrm{Re}(a^2) > 0. \end{aligned} \tag{B5}$$

Appendix C: Photoabsorption of SHG field

The strongest absorption channel is the absorption of SH field which is in resonance with $|0\rangle \to |1\rangle$ transition. To take into account this photoabsorption we need to add $-\mathbf{E}/2\ell$ at the right-hand side of paraxial equation (19)

$$\left(\frac{\partial}{\partial z} + \frac{1}{c}\frac{\partial}{\partial t} - \frac{\imath}{4k}\Delta_\perp\right)\mathbf{E} = -\frac{1}{2\ell}\mathbf{E} + \frac{\imath}{2k}\mathbf{f}, \tag{C1}$$

where $\ell = 1/\sigma N$ is the length of resonant absorption of the SHG field with the photoabsorption cross section σ. Using the substitution $\mathbf{E} = \tilde{\mathbf{E}}\exp(-z/2\ell)$ one can see that $\tilde{\mathbf{E}}$ satisfies paraxial equation (19)

$$\left(\frac{\partial}{\partial z} + \frac{1}{c}\frac{\partial}{\partial t} - \frac{\imath}{4k}\Delta_\perp\right)\tilde{\mathbf{E}} = \frac{\imath}{2k}\mathbf{f}e^{z/2\ell} \tag{C2}$$

with modified source term. This equation has the solution given by eq.(22) with $\mathbf{f}$ replaced by $\mathbf{f}\exp(z'/2\ell)$. Taking into account this we get immediately the solution of paraxial equation with photoabsorption (C1)

$$\mathbf{E}(z,\boldsymbol{\rho},t) = \tilde{\mathbf{E}}e^{-z/2\ell} = \frac{e^{-z/2\ell}}{2\pi}\int G(z-z',\boldsymbol{\rho}-\boldsymbol{\rho}',t-t')\mathbf{f}(z',\boldsymbol{\rho}',t')e^{z'/2\ell}dz'd\boldsymbol{\rho}'dt'. \tag{C3}$$

This means that to include the photoabsorption we should multiply by $\exp((z'-z)/2\ell)$ the integrand at the right-hand side of equations (25) for $J_\rho(z,\rho)$ and $J_z(z,\rho)$.

---

[1] N. Rohringer and R. London, Atomic inner-shell x-ray laser pumped by an x-ray free-electron laser, *Phys. Rev. A* **80**, 013809 (2009).

[2] N. Rohringer, D. Ryan, R. London, M. Purvis, F. Albert, J. Dunn, J. D. Bozek, C. Bostedt, A. Graf, R. Hill, S. P. Hau-Riege, and J. J. Rocca, Atomic inner-shell X-ray laser at 1.46 nanometres pumped by an X-ray free-electron laser, *Nature* **481**, 488-491 (2012).

[3] Y.-P. Sun, J.-C. Liu, and F. Gel'mukhanov, Slowdown and compression of a strong X-ray free-electron pulse propagating through the Mg vapors, *EuroPhys. Lett.* **87**, 64002 (2009).

[4] Y.-P. Sun, J.-C. Liu, and F. Gel'mukhanov, The propagation of a strong x-ray pulse followed by pulse slowdown and compression, amplified spontaneous emission and lasing without inversion, *J. Phys. B: At. Mol. Opt. Phys.* **42**, 201001 (2009).

[5] Y.-P. Sun, J.-C. Liu, C.-K. Wang, and F. Gel'mukhanov, Propagation of a strong x-ray pulse: Pulse compression, stimulated Raman scattering, amplified spontaneous emission, lasing without inversion, and four-wave mixing, *Phys. Rev. A* **81**, 013812 (2010).

[6] Q. Miao, J.-C. Liu, H. Ågren, J-E. Rubensson, and F. Gel'mukhanov, Dissociative X-ray Lasing, *Phys. Rev. Lett.* **109**, 233905 (2012).

[7] V. Kimberg and N. Rohringer, Amplified X-ray emission from core-ionized diatomic molecules, *Phys. Rev. Lett.* **110**, 043901 (2013).

[8] V. Kimberg and N. Rohringer, Stochastic stimulated electronic X-ray Raman spectroscopy, *Struct. Dynam.* **3**, 034101 (2016).

[9] V. Kimberg, A. Sanchez-Gonzalez, L. Mercadier, C. Weninger, A. Lutman, D. Ratner, R. Coffee, M. Bucher, M. Mucke, M. Agåker, C. Såthe, C. Bostedt, J. Nordgren, J.-E. Rubensson, and N. Rohringer, Stimulated X-ray Raman scattering: a critical assessment of the building block of nonlinear X-ray spectroscopy, *Faraday Discuss.* **194**, 305-324, (2016).

[10] M. Beye, S. Schreck, F. Sorgenfrei, C. Trabant, N. Pontius, S. Schüßler-Langeheine, W. Wurth, and A. Föhlisch, Stimulated X-ray emission for materials science, *Nature* **501**, 191-194 (2013)

[11] S. Tanaka and S. Mukamel, Coherent X-Ray Raman spectroscopy: A nonlinear local probe for electronic excitations, *Phys. Rev. Lett.* **89**, 043001 (2002).

[12] S. Mukamel, Multiple core-hole coherence in x-ray four-wave-mixing spectroscopies, *Phys. Rev. B* **72**, 235110 (2005).

[13] T. E. Glover, D. M. Fritz, M. Cammarata, T. K. Allison, S. Coh, J. M. Feldkamp, H. Lemke, D. Zhu, Y. Feng, R. N. Coffee, M. Fuchs, S. Ghimire, J. Chen, S. Shwartz, D. A. Reis, S. E. Harris, and J. B. Hastings, X-ray and optical wave mixing, *Nature* **488**, 603 (2012).

[14] N. Rohringer and R. Santra, Resonant Auger effect at high x-ray intensity, *Phys. Rev. A* **77**, 053404 (2008).

[15] J.-C. Liu, Y.-P. Sun, C.-K. Wang, H. Ågren, and F. Gel'mukhanov, Auger effect in the presence of strong x-ray pulses, *Phys. Rev. A* **81**, 043412 (2010).

[16] Y.-P. Sun, Q. Miao, A.-P. Zhou, R.-J. Liu, B. Liu, and F. Gel'mukhanov, Suppression of resonant auger effect with chirped x-ray free-electron laser pulse, *J. Phys. B: At. Mol. Opt. Phys.* **51**, 035602 (2018).

[17] P. Franken, A. Hill, C. Peters, and G. Weinreich, Generation of optical harmonics, *Phys. Rev. Lett.* **7**, 118-119 (1961).

[18] R. W. Boyd, *Nonlinear Optics*, Academic Press, Elsevier, Singapore, 2010.

[19] S. Shwartz, M. Fuchs, J. B. Hastings, Y. Inubushi, T. Ishikawa, T. Katayama, D. A. Reis, T. Sato, K. Tono, M. Yabashi, S. Yudovich, and S. E. Harris, X-Ray second harmonic generation, *Phys. Rev. Lett.* **112**, 163901 (2014).

[20] S. Yudovich and S. Shwartz, Second-harmonic generation of focused ultrashort x-ray pulses, *J. Opt. Soc. Am. B* **32**, 1894-1900 (2015).

[21] T. F. Heinz and D. P. DiVincenzo, Comment on "Forbidden nature of multipolar contributions to second-harmonic generation in isotropic fluids", *Phys. Rev. A* **42**, 6249-6251 (1990).

[22] M. O. Scully and M. S. Zubairy, Simple laser accelerator: Optics and particle dynamics, *Phys. Rev. A* **44**, 2656-2663 (1991).

[23] P. W. Milonni and J. H. Eberly, *Lasers Physics*, John Wiley & Sons, New York, 2010.

[24] L. Mandel and E. Wolf, *Optical Coherence and Quantum Optics*, Cambridge University Press, New York, 1995, p. 271.

[25] C. Buth, R. Santra, and L. Young, Electromagnetically induced transparency for X-rays, *Phys. Rev. Lett.* **98**, 253001 (2007).

[26] V. Schmidt, *Electron spectrometry of atoms using synchrotron radiation*, Cambridge University Press, Cambridge, England, 1997.

[27] C. Buth and R. Santra, X-ray refractive index of laser-dressed atoms, *Phys. Rev. A* **78**, 043409 (2008).

[28] J. L. Campbell and T. Papp, Widths of the atomic *K-N*7 levels, *At. Data Nucl. Data Tables* **77**, 1-56 (2001).

[29] M. Abramowitz and I. A. Stegun, eds., *Handbook of mathematical functions*, Dover, New York, 1965.

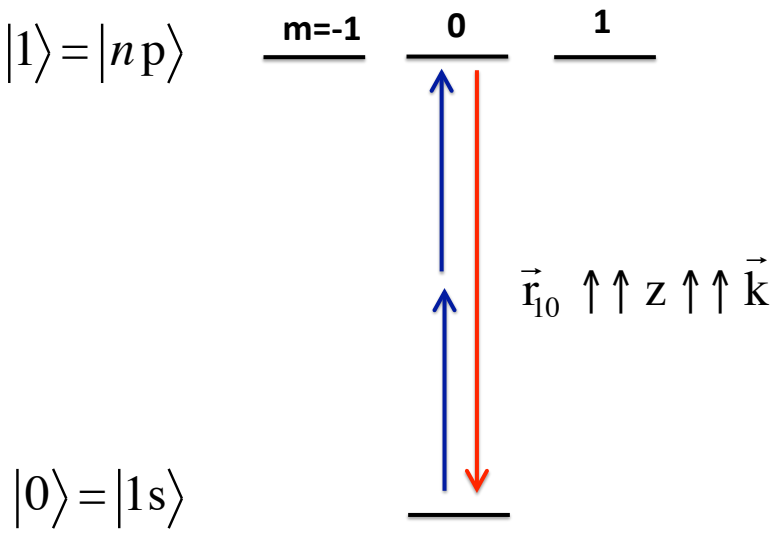

FIG. 1: The dipole moment $\mathbf{r}_{10}$ of the $1s \to np$ transition in atom is parallel to $\mathbf{k}$. The axis of quantization z is along the photon momentum $\mathbf{k}$.

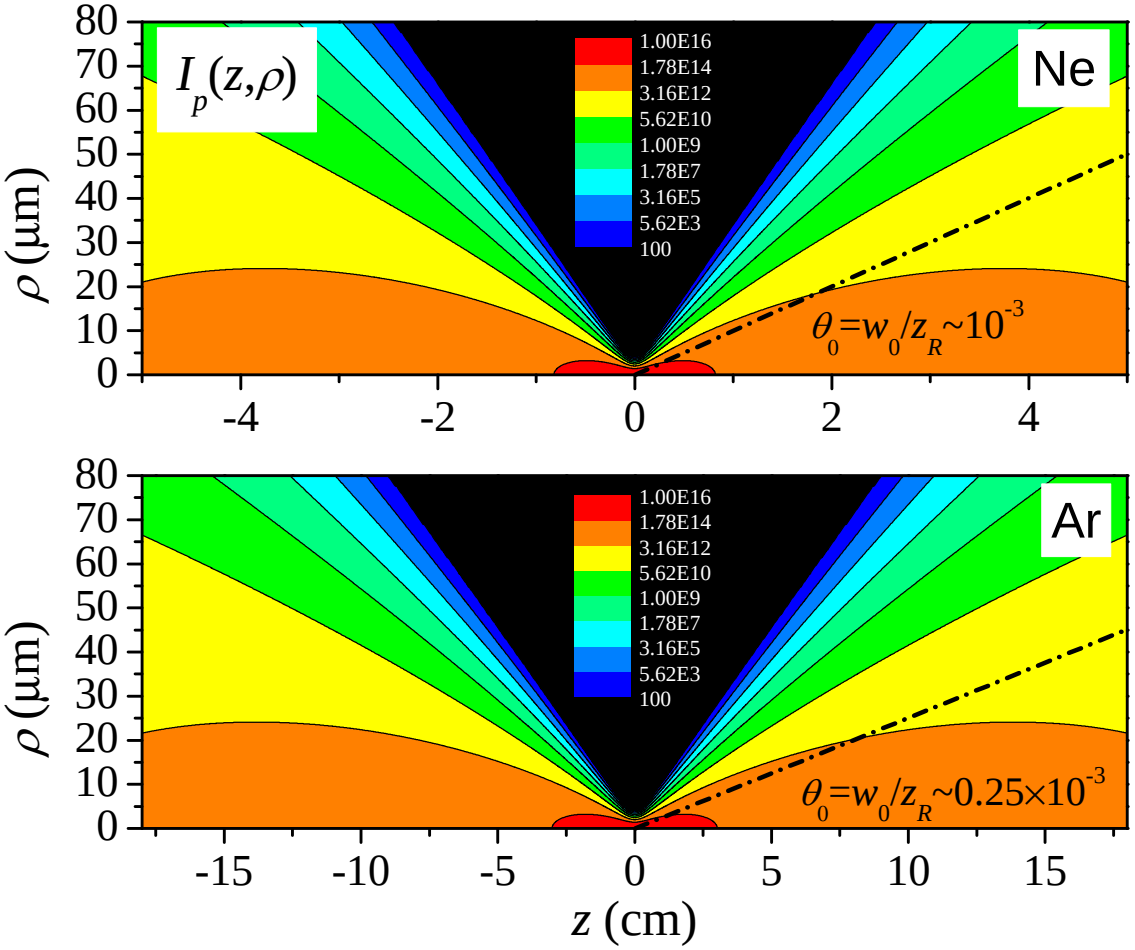

FIG. 2: 2D map of the pump intensity at $t = z/c$ for Ne and Ar atomic vapours. The legend shows the intensity in W/cm^2.

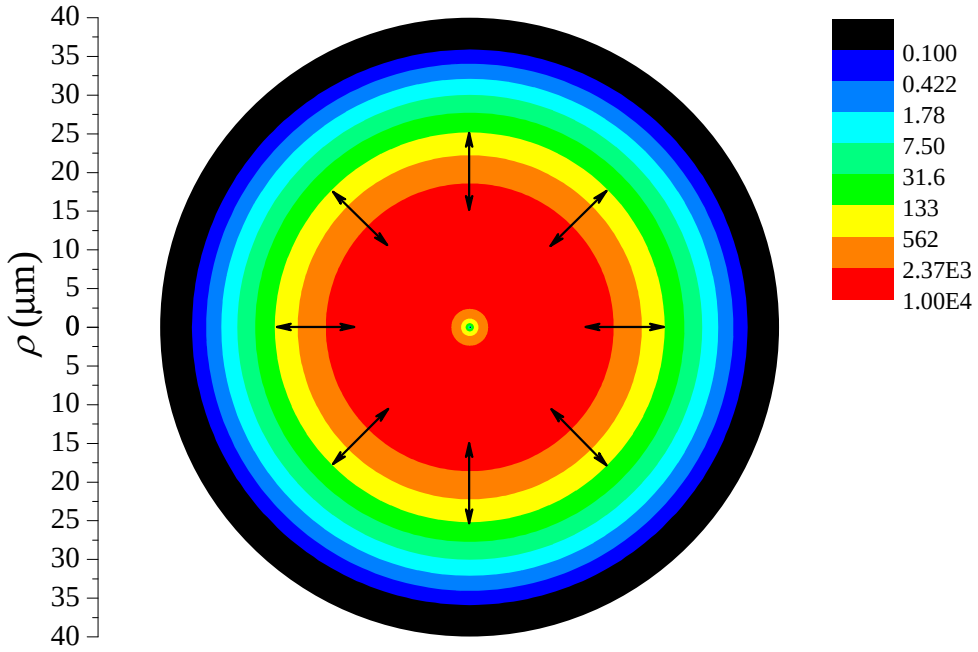

FIG. 3: Radial distribution of I_ρ for Ne atomic vapour at $z = 0.02$ m. Black arrows show schematically the radially polarized SHG field.

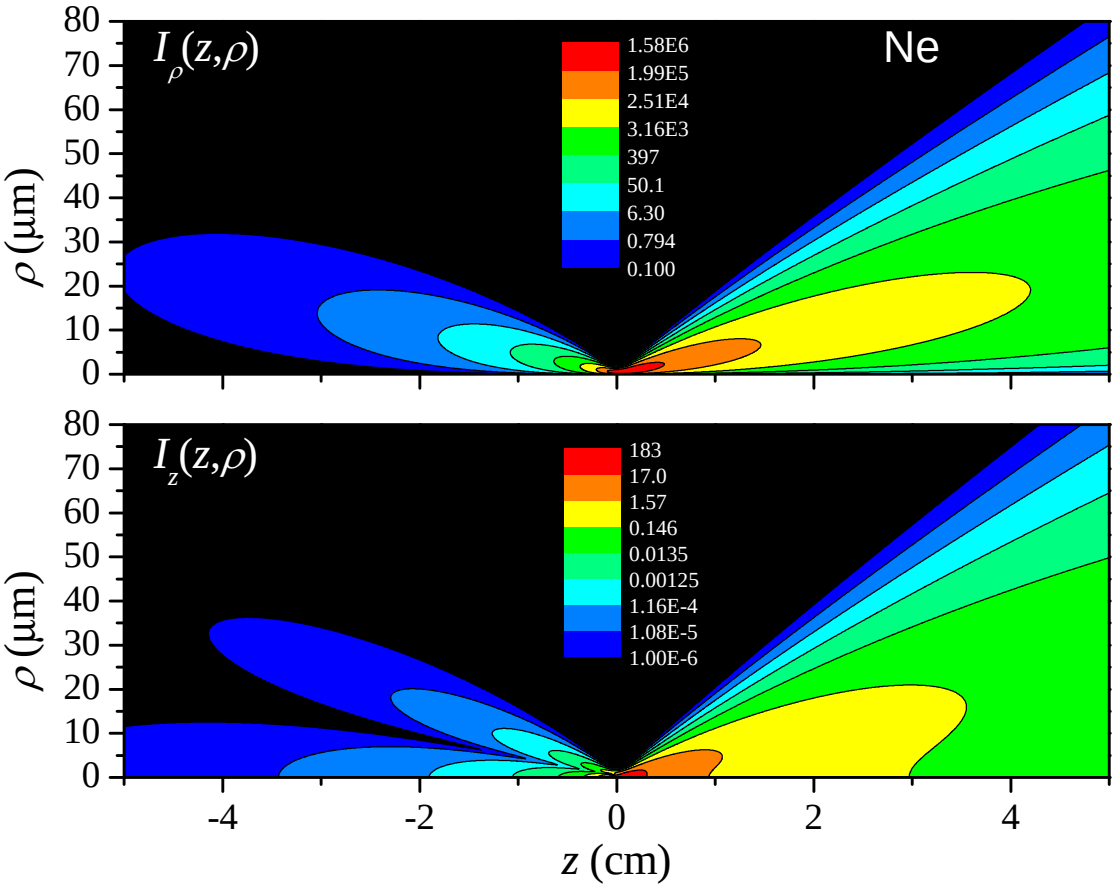

FIG. 4: 2D map of the SHG intensity at $t = z/c$ of Ne atomic vapour. The photoabsorption is negleted. The legend shows the intensity in W/cm^2.

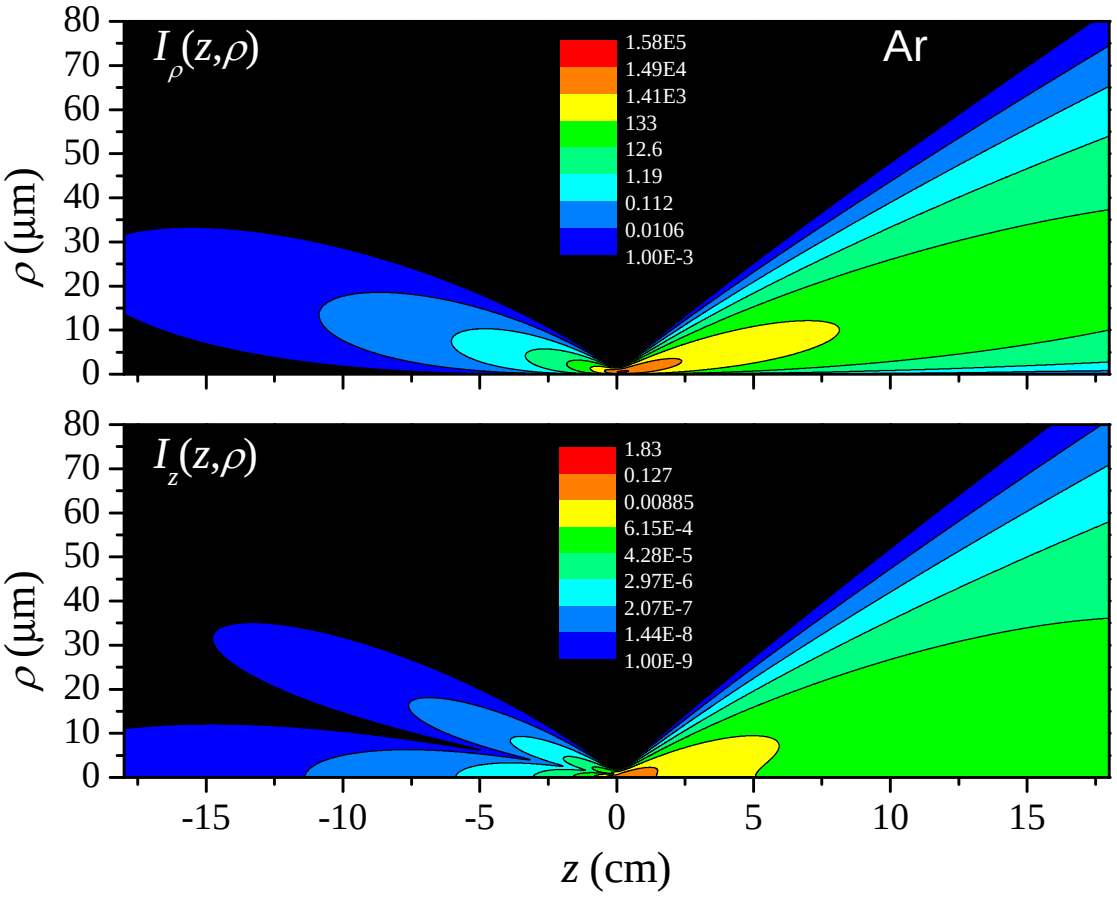

FIG. 5: 2D map of the SHG intensity at $t = z/c$ of Ar atomic vapour. The photoabsorption is neglected. The legend shows the intensity in W/cm^2.

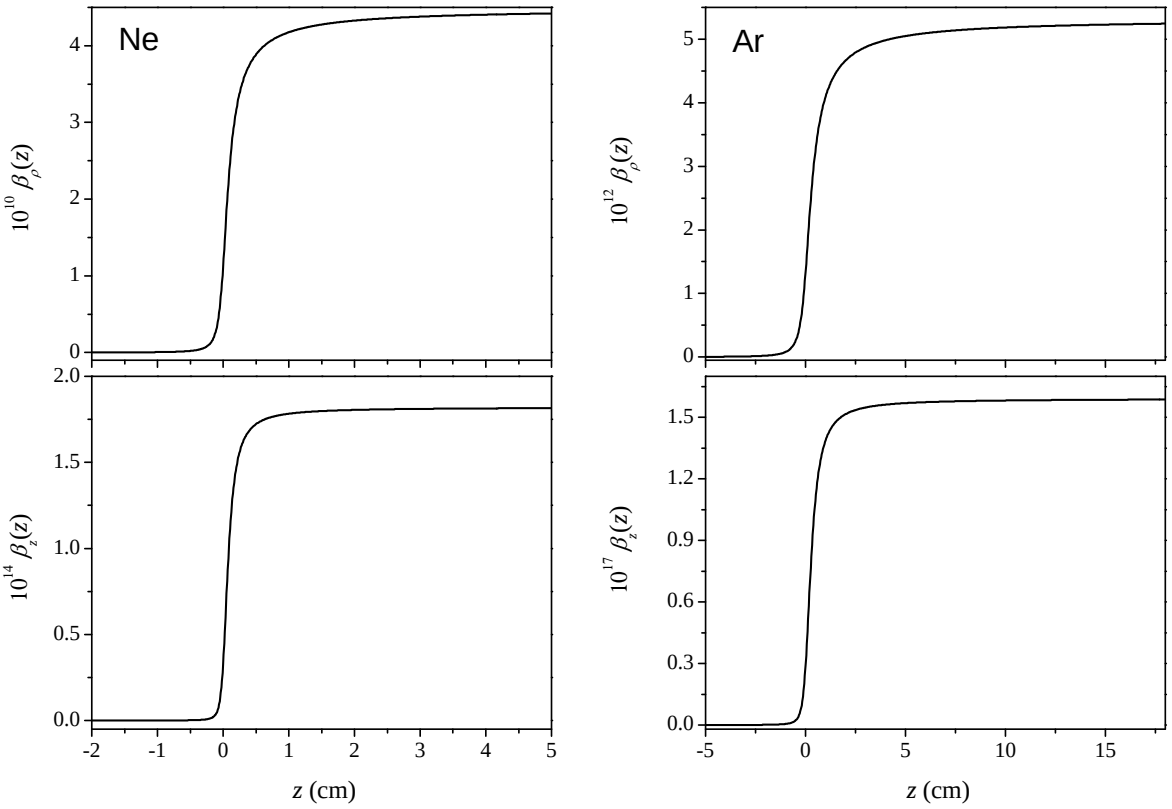

FIG. 6: Energy conversion efficiencies of the transverse SH fields $\beta_\rho(z)$ and the longitudinal SH fields $\beta_z(z)$ in Ne and Ar atomic vapours. The photoabsorption is neglected. The vertical axises show the energy conversion efficiencies multiplied by the factor 10^n: For example, $10^{10}\beta_\rho$ and $10^{14}\beta_z$ for Ne.

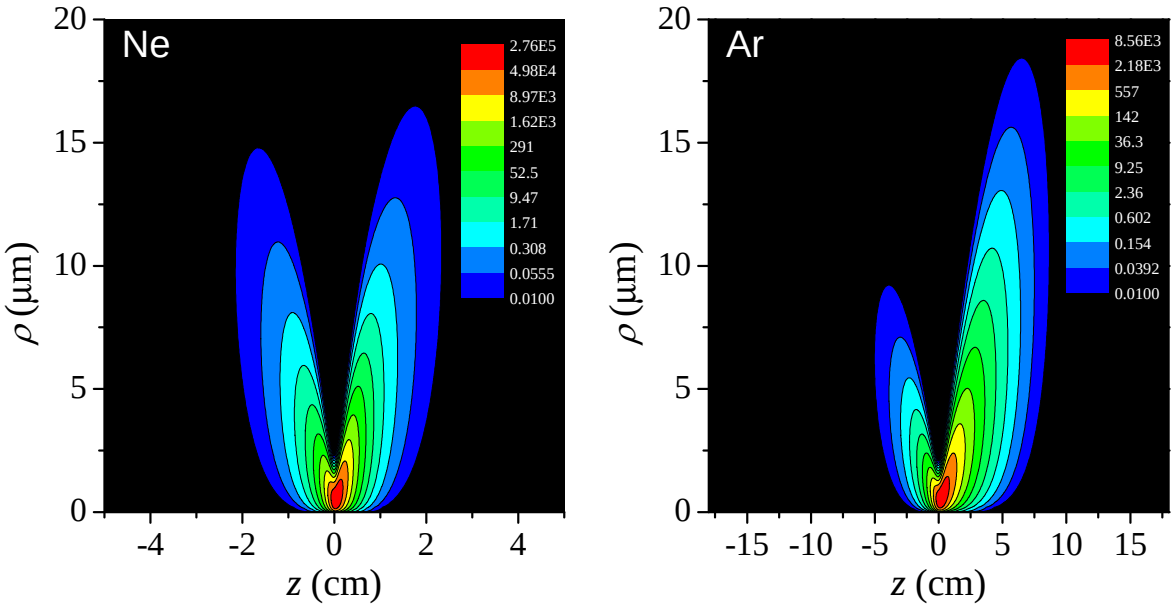

FIG. 7: Distribution of the transverse SH field I_ρ for Ne and Ar by taking into account the photoabsorption. The legend shows the intensity in W/cm^2.

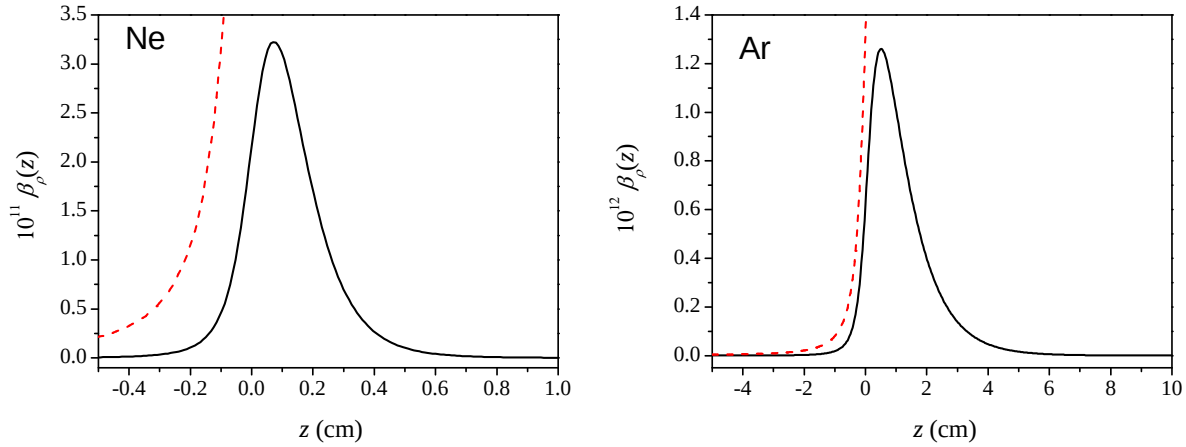

FIG. 8: Energy conversion efficiency $\beta_\rho(z)$ for Ne and Ar by taking into account the photoabsorption. The red dashed lines display $\beta_\rho(z)$ calculated by neglecting the photoabsorption (see Fig. 6). Ne: $\beta_\rho^{\max} = 3.2 \times 10^{-11}$ at $z_{\max} = 0.7$ mm. Ar: $\beta_\rho^{\max} = 1.3 \times 10^{-12}$ at $z_{\max} = 0.5$ cm.